INTERNATIONAL JOURNAL OF AUTOMOTIVE AND MECHANICAL ENGINEERING
ISSN: 2229-8649 e-ISSN: 2180-1606
VOLUME 22, ISSUE 3, 2025, 12725 - 12747
DOI: https://doi.org/10.15282/ijame.22.3.2025.15.0972

RESEARCH ARTICLE

Numerical Analysis of Enhanced Oil Recovery using Nanofluids

Krishna Priya* and Ahmed N. Oumer

School of Engineering and Physical Sciences, Heriot-Watt University, Dubai, United Arab Emirates

ABSTRACT – This study presents a comprehensive investigation into enhanced oil recovery (EOR) techniques utilizing nanofluids, specifically focusing on CuO, SiO_2, Al_2O_3, and TiO_2 nanoparticles. The objective was to develop a validated numerical model to assess the effectiveness of different nanofluids in EOR applications. The research methodology encompassed various pivotal stages. Initially, a meticulous selection process was employed to identify an appropriate base model for validation, ensuring accuracy and reliability throughout the study. Subsequently, nanofluids containing the aforementioned nanoparticles were selected, and their properties were characterized to enable accurate simulations. ANSYS Fluent, augmented with User-Defined Functions (UDF), was employed to simulate nanofluid displacement within the reservoir. Python and Minitab were used to support data analysis and validation. Mesh independence and saturation tests confirmed model stability. Key parameters such as velocity and interfacial tension were notably influential in affecting recovery performance. The RSM model predicted a theoretical maximum oil recovery of 105% for SiO_2 nanofluid under ideal conditions within the selected parameter range. Validation through saturation testing yielded an average recovery of 78.92%, closely matching the 75% reported in experimental studies. This demonstrates the model's strong potential as a predictive tool for optimizing nanofluid applications in real-world EOR operations.

ARTICLE HISTORY
Received : 10th Aug. 2024
Revised : 05th May 2025
Accepted : 03rd July 2025
Published : 22nd Sept. 2025

KEYWORDS
EOR
Nanoflooding
Nanofluid

1. INTRODUCTION

The historical importance of oil as a foundational energy source spans centuries, dating back to its discovery by the ancient Chinese in 600 B.C., initially transported through bamboo pipelines [1]. The inception of the modern oil and gas industry in 1847 marked a significant milestone in its evolution [2]. Oil production involves three stages: primary, secondary, and tertiary. Typically, only 15% to 40% of oil is recovered from the first two stages, with estimates varying among sources [3]. However, tertiary recovery shows potential in retrieving up to 75% [4] of previously untapped oil. This enhanced oil recovery (EOR) technique extends the life of oil fields, surpassing traditional methods and ensuring sustained production and increased returns on investments. Despite the maturity of conventional oil recovery methods, a significant proportion of oil remains unrecovered, necessitating advanced techniques to meet rising energy demands. The energy demand has been increasing throughout the years. EOR is one of the hydrocarbon technologies being applied in oil production. Strategies supporting EOR, such as Polymer EOR and Miscible Gas Flood, target barriers in implementing projects in the UK Continental Shelf (UKCS) [5]. Collaborative efforts aim to advance viable EOR methods. Acknowledged by the Department of Energy UK for its substantial employment contribution, this industry sustains a global workforce, crucial for supporting livelihoods [6]. Notably, oil meets an impressive 97% [7] of the UK's transport sector demand, highlighting its important role in maintaining vital transportation networks. Beyond transportation, oil serves as a fundamental element in producing a wide array of everyday goods, with refined oil byproducts forming the basis of various chemical products across diverse industries. Its enduring reliability as an easily stored energy source ensures a consistent and accessible supply, significantly contributing to its enduring relevance in the global energy landscape. EOR techniques play a pivotal role in extracting previously challenging or uneconomical oil reserves using conventional methods, especially chemical injection that involves mixing chemicals with fluids to enhance oil mobility toward production sites, like utilizing polymer solutions or Nanofluids for improved efficacy.

EOR explores Nanofluids, a method employing nanoparticles dispersed in a base fluid, often termed Nano-flooding. Widely utilized in the oil and gas industry, nanotechnology showcases versatility, enhancing equipment reliability, drilling, wastewater treatment, and notably, EOR, while emphasizing its eco-friendly nature [8]. Nanofluids attract attention due to their customizable thermo-physical and chemical attributes, prompting extensive research into their mechanisms and optimization for EOR, promising significant enhancements in recovery efficiency [9]. Overcoming limitations of conventional methods like water or surfactant flooding, Nanofluids offer advantages such as high oil recovery rates, stable pressure fluctuations, and minimal formation damage while enduring harsh reservoir conditions and modifying wettability at the immiscible fluid interface [10]- [12]. The use of Nanofluid flooding shows promising results for enhancing oil recovery in reservoirs [13] [14]. The results from Ragab and Hannora [15], based on the size of the nanoparticle, agree with those obtained by Jiang et al. [16]. The researchers Jiang et al. investigated the impact of various sizes of silica nanoparticles, including 10, 40, 90, and 150 nm, on wettability changes. The results revealed that smaller

*CORRESPONDING AUTHOR | **Krishna Priya** | ✉ krishnapriya1998@gmail.com

nanoparticles caused a more significant shift in wettability, resulting in higher oil recovery [16]. Therefore, it can be said that the application of smaller nanoparticles was found to be more effective in enhancing oil recovery. From the study by Khan et al., it is observed that for nanoparticles under the same concentration and base solution, SiO_2 nanoparticles for the same injected pore volume provide a slightly higher percentage of oil recovery compared to Fe2O3 and TiO_2 [17]. TiO_2 provided a lesser percentage of oil recovery for the same volume [17]. According to a study by Ragab and Hannora [15], the recovery factor of nanofluid using silica nanoparticles at 0.1 wt% increased the recovery factor by 11%. Using nanofluid with aluminum oxide nanoparticles at 0.1 wt% resulted in a decrease of the recovery factor by 8%. The probable reason for this is due to the poor suspension of material in the brine. While these studies offer valuable insights into the effects of different nanoparticles, a critical analysis reveals that most focus on isolated parameters such as particle size or type without exploring the interplay between multiple factors. Additionally, inconsistencies in experimental conditions across studies make direct comparison difficult and limit broader generalizations.

The research by P. Rostami et al. [18] on the exploration of diverse pore structures and their impact on oil recovery using nanofluid flooding represents a significant step in understanding EOR techniques. It unveils the potential benefits of random pore distribution and the integration of nanoparticles in improving oil recovery rates. The study's focus on controlled experiments may require further investigation in real-world reservoirs to validate the applicability of these findings. Exploring a wider array of influencing factors beyond pore structures and nanoparticles could provide a more comprehensive understanding of effective oil recovery strategies. These initial findings offer promising insights that could revolutionize oil recovery methodologies with further refinement and practical validation.

The type of nanoparticles, size and pore morphology are important factors that have been widely studied. The studies done in the literature are generally theoretical. Laboratory experiments and on-site pilot tests are carried out to explore the use of nanoparticles as EOR modifiers to change the wettability of rocks and the interfacial tension between oil and injected fluid. Numerous pilot tests and field applications have been conducted lately across the world [13], [19]- [21], despite some uncertainties regarding the use of nanoparticles for improving oil recovery. Promising results have been observed in oilfields such as Henan, Daqing, Jiangsu, and Shengli in China, based on field experiments [10]. Together, these findings from both lab and field studies suggest a promising direction for Nano-EOR yet also indicate variability in effectiveness depending on nanoparticle type, reservoir conditions, and injection strategies — underscoring the need for integrated evaluations. Although nanoparticle EOR methods have been used in field-scale projects in some oilfields, they are still relatively new and immature compared to traditional EOR methods such as water, gas, and polymer flooding. The usage of Nanofluids for EOR represents a novel application of nanotechnology in the oil and gas industry, which can contribute to innovation and the development of new technologies. Therefore, a comprehensive investigation is required to determine the optimal use of nanoparticle EOR methods from various perspectives.

The paper by A. Ali and B. Salam [22] provides a comprehensive overview of nanofluids' potential in enhancing heat transfer, highlighting their remarkable thermal conductivity and rheological properties. It examines previous studies and recent advancements, focusing on nanofluid preparation, stability enhancement, and the influence of factors like particle size, shape, and temperature on thermal conductivity. By showcasing potential applications in various fields, from electronics cooling to solar energy and desalination, the paper emphasizes the versatility of nanofluids. To better understand the intricate dynamics, a simulation project could be instrumental. Simulations could delve into the complex behavior of nanofluids in diverse scenarios, providing insights that may not be easily obtainable through experimental studies alone. This approach could pave the way for overcoming current challenges and optimizing nanofluid applications for more efficient heat transfer across industries.

A recommendation proposed by Iravani et al. for future studies in the same field includes simulation and modelling studies to provide valuable insights into the effectiveness of EOR methods [19]. Simulation and modelling studies have advantages over other types of studies. They are generally affordable and expeditious. Through simulation, it is possible to visualize the flow in any aquifer or reservoir without the use of sophisticated cameras. Numerous runs can be conducted swiftly and safely. They provide a controlled environment that allows the manipulation of variables, repetition of scenarios, and exploration of diverse outcomes without any ethical concerns. However, there is currently a shortage of adequate simulation and modelling studies, particularly for the widespread implementation of nanoparticles in EOR. Despite the growing body of research on nanoparticle-assisted EOR, there is a noticeable lack of comprehensive modelling studies that bridge experimental findings with large-scale reservoir simulation, leaving a gap in understanding their practical, field-level applicability. To address this gap, the present study aims to develop a numerical model to simulate the EOR process using Nanofluids, providing insight into their behavior in porous media. This simulation-based approach is intended to complement existing experimental studies by offering a cost-effective and safe way to analyze parameter variations. The findings can guide future field applications and contribute to optimizing EOR strategies involving nanotechnology. The novelty of this work lies in its integration of numerical simulation with statistical optimization to systematically evaluate and identify the most effective nanoparticle-assisted EOR conditions — an area that remains relatively underexplored. The objectives of this study are as follows:

- To create a numerical model and investigate the oil recovery rate using Nanofluids.
- To determine the best combination of process parameters for maximum oil recovery rate using statistical methods.

2. SELECTION OF BASE MODEL

Model validation is a critical aspect of ensuring the accuracy and reliability of simulations or models used in various fields like engineering, physics, biology, and more. The Finite Volume Method (FVM) establishes that the numerical simulations accurately represent the physical behavior of the system being studied. The process involves comparing simulation results with experimental or analytical data to assess the reliability and accuracy of the finite volume model. When discussing validation, establishing a base model plays a pivotal role in the validation of any model. The paper by M. Q. Alsedrani [23], serves as a valuable reference for understanding the impact of silica nanofluids on EOR through Computational Fluid Dynamics (CFD) simulations. This paper presents a comprehensive investigation into the utilization of silica nanofluids, focusing on their effects and potential applications in the realm of EOR. Alsedrani's work offers a structured exploration of the behavior and performance of silica nanofluids in enhancing the recovery of oil from reservoirs. M. Q. Alsedrani's research, specifically chosen for its alignment with the current experiment's objectives and comprehensive detailing, builds upon a model developed by Rostami et al. [24]. This choice enhances its relevance to Alsedrani's research goals. Rostamani et al's paper showcases promising experimental outcomes regarding the use of silica nanofluids to enhance oil recovery. Notably, the simulation software used in both papers aligns with the software intended for use in the present experiment, leveraging established research to authenticate and potentially augment the findings.

3. SOFTWARE

In this project, three main software were used, namely: Ansys Fluent, Minitab, and Python.

ANSYS Fluent, a leading computational fluid dynamics software, plays a pivotal role in the numerical analysis of nano flooding. Nanofluids exhibit intricate behaviors that require detailed examination. Fluent's capabilities enable the simulation and understanding of these complexities, including the flow dynamics, heat transfer characteristics, and interactions within nanofluids. This software facilitates the prediction of nanofluid behaviors, aiding in optimizing their applications across diverse fields such as cooling systems, biomedical devices, and energy applications. Following the acquisition of data from Ansys Fluent, the next step involves utilizing programming language software. Python, a versatile programming language, offers a wide array of benefits. Python's libraries like Pandas, NumPy and Matplotlib enable efficient data analysis, manipulation and visualization, empowering users to extract crucial insights from their datasets effortlessly. Its readability and simplicity enable the automation of repetitive tasks, saving time and effort in project workflows. What makes Python especially appealing is its open-source nature, ensuring cost-effectiveness while catering to diverse needs. The broad community support further solidifies Python's position, providing users with a robust platform backed by ample resources and expertise, making it an indispensable choice for project endeavors. Following the use of numerical simulation software and programming languages to facilitate data analysis and optimize values, a statistical tool known as Minitab is employed. Minitab serves as a pivotal tool for embarking on projects by offering robust statistical analysis capabilities. Its user-friendly interface serves as a catalyst for informed decision-making, offering capabilities to analyze data trends, identify areas for quality improvement, and conduct comprehensive statistical analyses. Its diverse array of statistical methods, encompassing hypothesis testing, regression analysis, and design of experiments, empowers users to extract actionable insights from their data. Additionally, Minitab's visualization tools and customizable reporting features facilitate clear communication of findings, aiding in the tracking of progress and driving impactful changes.

4. PHYSICAL DOMAIN & COMPUTATIONAL DOMAIN

The study's precision in constructing geometric representations drew inspiration from Y. Zhou et al.'s paper [25], which employed the Fourier series method to replicate irregular sand grain shapes identified in rock samples meticulously. Y. Zhou et al.'s methodology involved detailing grain contours across different coordinate systems, enabling the creation of digital models mirroring the observed irregularities in real sand grains. This approach, akin to Clark's [26] and Su and Yan's [27] techniques, elaborated on grain contours in local and global coordinate systems using the Fourier series, facilitating the generation of 2D irregular grains. These methods, including discretization, mapping parametric curves, and achieving targeted porosities, were integral in creating accurate digital models of porous media. The validation of these digital grain models was pivotal. The comparison of 50 randomly selected grains' characteristics with 100 natural sand grains affirmed the close resemblance, confirming the accuracy of the digital representation in replicating real sand grain irregularities observed in rock samples. Despite differing core samples and approaches between the papers by Y. Zhou et al. [25] and Y. Ahmadi et al. [28], the shared porosity values serve as a unifying factor. This parallel indicates a commonality in the porosity of the materials studied, aligning the digitally created models from Y. Zhou et al.'s work with the porosity characteristics observed in the cores examined by Y. Ahmadi et al. [28].

Validation requires benchmarking the numerical solution against analytical or experimental data. Comparing simulated pressure profiles, temperature distributions, and nanoparticle concentrations with known solutions ensures that the chosen governing equations accurately represent the physical processes occurring in the reservoir. The validation process for the constructed model involved creating the geometry based on a referenced paper. In the referenced study by P. Rostami et al. [24], a micromodel network was crafted using design software and etched onto a glass plate. This model mimicked a porous network, detailing specific channel depths, grain sizes, porosity, and throat sizes. Before testing, the micromodel underwent thorough cleaning and preparation. The experiments involved three types of flooding tests: water

injected into water-wet and oil-wet systems, and nanofluid injected into oil-wet systems. Each test followed a three-step process: saturating with water, injecting oil, and subsequent flooding with water and nanofluid. Throughout the experiments, digital imaging and video recording were used, and image quality was enhanced through specialized software. ImageJ software was utilized to determine phase saturations, while the percentage of initial oil-in-place (IOIP) represented the measured oil recovery. The experimental setup included a syringe pump for fluid injection, a high-resolution camera for video recording, and backlighting for better imaging. This research aimed to comprehend how oil displaces under different conditions and to assess recovery rates using the intricately designed micromodel.

The process of creating the reservoir's geometry for nano flooding simulation in EOR involves replicating the reservoir's actual characteristics through a model. This can be achieved using CAD software such as SolidWorks, Autodesk Inventor, or directly within the ANSYS software suite, particularly the powerful geometric design tools like ANSYS Fluent Design Modeler or ANSYS Space Claim. These platforms facilitate precise delineation of the reservoir's boundaries and integration of crucial components like wells and injection points, ensuring an accurate representation that mirrors real-world conditions. For this study, the reservoir geometry emulates the model utilized in Y. Zhou et al.'s experiment [25], portraying a two-dimensional homogeneous porous structure as shown in Figure 1. M. Q. Alsedrani's experiment [23], portraying a two-dimensional porous structure measuring 4cm in width and 6cm in length, with a grain size of 1.48 and a porosity level of 0.34, as shown in Figure 2, is used for the validation. This detailed geometric representation serves as the foundation for simulating nano flooding processes in EOR, aiming to replicate real reservoir behavior under these specific conditions.

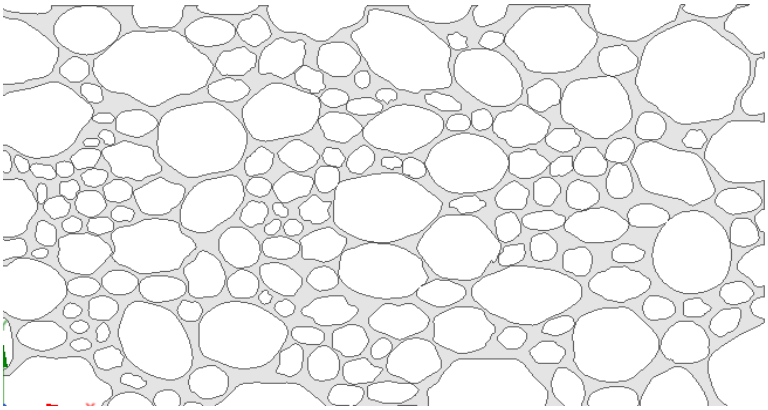

Figure 1. Geometry of the proposed model

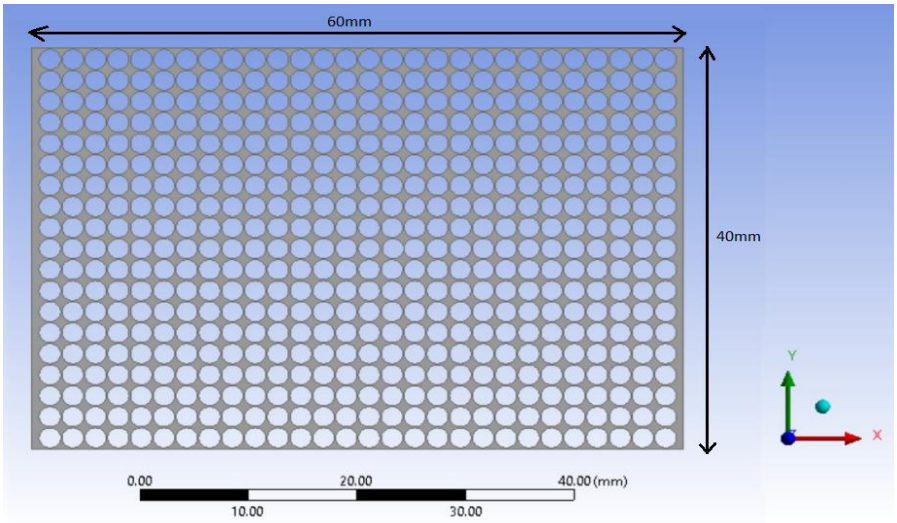

Figure 2. Geometry used for model validation

5. MESHING

Meshing, the process of discretizing the geometry into finite elements, significantly influences simulation accuracy. A well-designed mesh captures the intricate details of the reservoir, ensuring a precise representation of fluid flow and nanoparticle transport. The software offers various meshing tools and techniques to accomplish this task efficiently. The face meshing is employed for the 2D model to efficiently discretize the surface into smaller elements. This method is advantageous as the analysis primarily focuses on surface interactions, and a full 3D representation is unnecessary for the selected model. Face meshing offers computational efficiency by reducing complexity, resulting in quicker computations

and lower memory requirements. It allows for more accurate capture of boundary conditions and gradients along the surface, making it suitable for simulations where key phenomena occur predominantly at the boundaries. It is crucial to use face meshing in scenarios where the analysis is inherently two-dimensional. ANSYS Fluent meshing capabilities extend to automatic mesh generation, which streamlines the process by allowing users to define specific parameters for mesh density, refinement, and quality criteria. Quality checks play a crucial role in ensuring the reliability of the mesh. ANSYS Fluent offers comprehensive tools to assess element quality, boundary conformity, aspect ratios, skewness, and other criteria necessary for accurate simulations. The mesh can be modified based on these assessments to achieve the desired balance between accuracy and computational efficiency. The quality of all the meshes generated was within the optimal range, ensuring that the mesh generated was of good quality.

6. GOVERNING EQUATIONS

6.1 Continuity

The conservation of mass inside the fluid domain is expressed by the continuity equation, which is expressed as the net flow rate of mass into or out of a control volume equals the rate of change of mass inside the control volume.

$$\frac{\partial p}{\partial t} + \nabla \cdot (\rho u) = 0 \tag{1}$$

where, p is the pressure, ρ is the fluid density and u is the fluid velocity vector.

6.2 Momentum

The following equations explain the conservation of momentum inside the fluid. It considers the pressure, outside forces, and viscous effects into account and is composed of the momentum conservation equation and the viscous stress tensor. In the context of the assumptions made for the model, the momentum equation becomes:

$$\frac{\partial(\rho u)}{\partial t} + \nabla \cdot (\rho u u) = -\nabla p + \nabla \cdot \left(\mu(\nabla u + \nabla u^T)\right) + f \tag{2}$$

where μ is the dynamic viscosity, T provides the matrix transpose and f represents external forces like gravity.

6.3 Volume of Fluid Model

The tracking of the interface(s) between the phases is done by solving (1) for the volume fraction of the phases. For the q^{th} phase, the continuity equation is given by [29]:

$$\frac{1}{\rho_q}\left[\frac{\partial}{\partial t}\left(\alpha_q \rho_q\right) + \nabla \cdot \left(\alpha_q \rho_q \overrightarrow{v_q}\right) = S_{\alpha_q} + \sum_{p=1}^{n}\left(\mathrm{rh_{pq}} - \mathrm{rh_{qp}}\right)\right] \tag{3}$$

α_i is the q^{th} fluid's volume fraction and is defined as the following [29]:

$$\alpha_i = \begin{cases} \alpha_i = 0 & \text{the cell is empty} \\ 0 < \alpha_i < 1 & \text{the cell contains the interface} \\ \alpha_i = 1 & \text{the cell is full of i}^{\text{th}}\text{ fluid} \\ \sum_{p=1}^{n} \alpha_p = 1 & \text{the cell is filled with either single fluid phase or a combination} \end{cases} \tag{4}$$

With this definition for phase, (3) becomes:

$$\frac{\partial \alpha_i \rho_i}{\partial t} + \nabla \cdot (\alpha_i \rho_i u) = \rho_i S_{\alpha_i} + \sum_{j=1}^{n}\left(rh_{ji} - rh_{ij}\right) \tag{5}$$

where rh_{ij} describes the mass transfer between i and j. In the simulation, both rh_{ij} and rh_{ji} is zero since there is no mass transfer assumption between water and oil in the model. $S_{\alpha q}$ is the source of the ith fluid, ρ_i is the density and u is the velocity vector. In an n-phase system, the volume fraction averaged density and viscosity are taken as [23]:

$$\begin{cases} \rho = \sum \alpha_i \rho_i \\ \mu = \sum \alpha_i \mu_i \end{cases} \quad \text{averaged over an n-phase system} \tag{6}$$

The volume fraction is not solved for the primary phase, in this case, oil. It is computed based on the following constraint:

$$\sum_{q=1}^{n} a_k = 1 \tag{7}$$

6.4 Wall Adhesion

To alter the contact angle between the two phases with the solid interface (wall), the wall adhesion model was chosen for the VOF model. This surface near wall adjustment is created mathematically using the following equation [23]:

$$\hat{n} = \hat{n}_w cos\theta_w + \hat{t}_w sin\theta_w \quad (8)$$

where, $\hat{n}_w$ is the unit vector normal to the wall and $\hat{t}_w$ is the unit vector tangential to the wall.

6.5 Thermal Conductivity

For calculating the Thermal Conductivity of the nanofluid, the following equation is used [23]:

$$k_{\text{nf}} = (4.97\varphi^2 + 2.72\varphi + 1)k_{\text{bf}}$$

where φ is the concentration of nanofluid and k_{bf} is the thermal conductivity of the base fluid.

6.6 Density

For calculating the Density of the nanofluid, the following equation is used [23]:

$$\rho_{\text{nf}} = (1 - \varphi)\rho_{\text{bf}} + \varphi\rho_{\text{b}}$$

where, ρ_{bf} is the density of the base fluid and ρ_{b} is the density of the nanoparticles.

6.7 Specific Heat

For calculating the Specific Heat of the nanofluid, the following equation is used [23]:

$$C_{\text{nf}} = \frac{\left((1 - \varphi)\rho_{\text{bf}}C_{\text{bf}}\right) + \varphi\rho_{\text{b}}C_{\text{b}}}{\rho_{\text{nf}}}$$

where, C_{bf} is the Specific Heat of the base fluid and C_{b} is the Specific Heat of the nanoparticles.

6.8 Viscosity

For calculating the Viscosity of the nanofluid, the following equation is used [23]:

$$\mu_{\text{nf}} = \mu_{\text{bf}} \times \left(1 - \frac{\varphi}{\varphi m}\right)^{-\eta\varphi m}$$

where μ_{bf} is the viscosity of the base fluid, and φm is assumed to be 0.5, and η is assumed to be 2.5 in (5).

7. NANOFLUID PROPERTIES

The nanofluid used in the validation is silica nanoparticles suspended in synthetic seawater. The fluid properties were considered corresponding to the experiment and simulation [23] [24]. The viscosity and density of the nanofluid with 0.2% concentration of silica nanoparticles were measured experimentally. The properties of silica nanoparticles, base fluid, and oil, along with other nanofluids used for the proposed model, are shown in Tables 1-6.

Table 1. Properties of base fluid [23]

Property	Unit	Value
Density	Kg/m^3	1040
Specific Heat	J/kg.K	4182
Thermal Conductivity	W/mK	0.6
Viscosity	kg/ms	0.001003

Table 2. Properties of crude oil [23]

Property	Unit	Value
Density	Kg/m^3	875
Specific Heat	J/kg.K	2420
Thermal Conductivity	W/mK	0.147
Viscosity	kg/ms	0.0177
Molecular Weight	kg/kmol	114.1502
Latent Heat	J/kg	306.446
Droplet Surface Tension	dynes/m	0.02123

Table 3. Properties of SiO_2 nanoparticle [23]

Property	Unit	Value
Density	Kg/m^3	2200
Specific Heat	J/kg.K	745
Thermal Conductivity	W/mK	1.4
Viscosity	kg/ms	20

Table 4. Properties of CuO nanoparticles [30]

Property	Unit	Value
Density	Kg/m^3	6310
Specific Heat	J/kg.K	531
Thermal Conductivity	W/mK	20
Viscosity	kg/ms	30

Table 5. Properties of Al_2O_3 nanoparticle [31]

Property	Unit	Value
Density	Kg/m^3	3970
Specific Heat	J/kg.K	765
Thermal Conductivity	W/mK	40
Viscosity	kg/ms	40

Table 6. Properties of TiO_2 nanoparticle [32]

Property	Unit	Value
Density	Kg/m^3	4000
Specific Heat	J/kg.K	690
Thermal Conductivity	W/mK	11
Viscosity	kg/ms	50

Following the equations in section VI of specific heat and thermal conductivity, which provide an estimation of the nanofluid properties, the user-defined function in Fluent was used to input the required properties. In Ansys Fluent, a User Defined Function (UDF) represents a customized subroutine or function that users develop to define specific behaviors or conditions not inherently available within the standard Fluent software package. UDFs serve the purpose of implementing bespoke equations, boundary conditions, material properties, or other user-defined features within the Fluent solver. These functions are typically authored in programming languages such as C, C++, or Fortran and subsequently compiled into shared libraries. These libraries are then utilized by Fluent during simulations. UDFs offer users the flexibility to extend Fluent's capabilities beyond its native functionalities, enabling the execution of complex simulations and tailored customizations aligned with specific requirements or objectives.

8. ANSYS FLUENT SETUP

Ansys offers varied solver options: the pressure-based solver for incompressible flows, iteratively solving pressure and velocity fields, and the density-based solver for compressible flows with density variations. Velocity formulations include absolute (global frame) and relative (specified frame) options. 2D space selections simplify computations: planar, axisymmetric, or axisymmetric swirl. Planar simulations assume flow occurs in a single plane, axisymmetric simulations consider rotational symmetry around an axis, while axisymmetric swirl combines axisymmetric geometry with swirling flow. Each simplifies computations based on different symmetrical characteristics in geometry and flow behavior. These options reduce computational complexity while capturing dominant flow characteristics.

Steady simulations assume constant flow conditions, suitable for stable systems where flow remains unchanged. These simulations simplify computations by assuming a steady-state condition throughout. On the other hand, the transient simulations model changes over time, capturing time-dependent behavior in the system. They are used for scenarios where flow conditions vary dynamically, providing detailed temporal information. Gravity impacts flow patterns and pressure distribution, especially in vertical or inclined scenarios. Homogeneous models simplify phase interactions, and inhomogeneous models allow non-uniform properties. Volume fraction handling (implicit/explicit) influences computational efficiency. Additional aspects include implicit body forces, anti-diffusion measures, and interface modelling. Viscous models encompass turbulence (k-epsilon, k-omega) and laminar simulations. Solution methods (SIMPLE, SIMPLEC, PISO, Coupled) handle pressure-velocity coupling. Numerical schemes, convergence criteria, time

step sizes, and iterations ensure solution accuracy and stability. Proper initialization sets simulation foundations. Detailed understanding and adjustments are crucial for precise simulation outcomes in Ansys Fluent.

9. METHODOLOGY

The simulation model was structured with specific assumptions to replicate the nano-flooding dynamics essential for EOR accurately. Initially, the model assumed complete saturation of crude oil, denoted as 100% (Swi=0), representing the reservoir's initial state. Two-phase flow conditions were implemented, designating crude oil as the primary phase (representing the displaced fluid) and nanofluid as the secondary phase (the injected fluid). The micromodel flooding in the simulation was carried out at ambient temperature as used in the experiment [23]. Additionally, constant pressure conditions were maintained, ensuring the simulation closely emulated the natural environment of reservoirs. Dynamic transient state conditions were implemented, enabling the simulation to study displacement mechanisms over time. This unsteady time approach, utilizing transient state conditions, allowed for a comprehensive analysis of how the injected nanofluid displaced the crude oil within the reservoir model.

The injection flow rate remained constant throughout the simulation, ensuring consistency in the injection process. To model the fluid flow within the reservoir, laminar flow conditions were chosen, employing a consistent inlet velocity of 0.004 m/s. This velocity was selected deliberately to displace crude oil effectively at the pressure outlet while maintaining the flow regime within the laminar region. Keeping Reynolds's number within the laminar range ensured stability and accuracy in the simulation results, enabling a more precise examination of the displacement process without turbulent effects. The interfacial tension between the crude oil and nanofluid was set at 0.015 N/m, a pivotal factor influencing the interaction and displacement dynamics between these fluids within the reservoir. Leveraging experimental data, the contact angle at the solid surface and water phase was established at 50°. This angle played a significant role in determining the wetting properties, impacting how the injected fluid interacts within the reservoir rock matrix.

In ANSYS Fluent, under-relaxation factors are numerical parameters used to control the convergence behavior of iterative solvers. They regulate the influence of the current iteration's solution on the subsequent iteration, affecting how quickly the solution converges to a stable state. These factors are crucial in fine-tuning the convergence process, particularly when solving complex fluid flow, heat transfer, or structural problems. Fluent employs various under-relaxation factors for different variables such as velocity, pressure, turbulence parameters, and more. Adjusting these factors can impact the stability, speed, and accuracy of convergence in simulations. By modifying these factors within ANSYS Fluent, engineers and researchers can tailor the convergence behavior to achieve accurate and efficient simulation results, balancing the trade-off between computational efficiency and solution accuracy. Notably, the simulation focused solely on displacement phenomena, excluding considerations for heat transfer. This focused investigation allowed for a deeper understanding of displacement mechanisms.

In ensuring result accuracy, each flooding case's flow time persisted until a critical point: the absence or negligible further displacement of crude oil by the injected fluid. The simulation was conducted with a time step (Δt) of 1 second, enabling a precise temporal resolution of the displacement process. Additionally, a maximum iteration limit of 3000 iterations was established, ensuring computational efficiency without compromising result fidelity. The choice of a substantial iteration count in this context is conducive to achieving a detailed and accurate representation of the displacement dynamics. The saturation point, a pivotal milestone in the simulation, was reached within 20 timesteps. Saturation is defined as the state where either no further displacement of crude oil occurred or was exceedingly minimal due to the injected fluid. This saturation criterion served as a reliable indicator of the displacement process's completion, marking a critical stage in assessing the efficiency of the nano flooding strategy for EOR within the simulated reservoir context. Python scripting was employed for preprocessing tasks such as parameter assignment and automated result extraction, as well as for postprocessing tasks like calculating oil recovery and tracking saturation changes. Additionally, Minitab was used to analyze trends in recovery efficiency, supporting statistical interpretation of the simulation outcomes.

9.1 Saturation Test

A crucial saturation test was conducted, focusing on a specific mesh size to validate the discernibility of saturation through visual representation. The chosen mesh size of 0.2 mm allowed for a more detailed observation of the simulation dynamics. The saturation verification primarily relied on the animation depicting volume fraction changes of oil at various time steps, as shown in Figure 3. This visual representation served as a powerful tool in discerning saturation dynamics within the reservoir model.

Table 7. Saturation test

Contact Angle	Duration	Efficiency
50°	17s	77.45%
50°	18s	77.55%
50°	19s	77.29%
50°	20s	77.47%
50°	30s	76.83%
50°	120s	77.53%

Notably, the examination of the data revealed an intriguing observation: the recovery percentage exhibited minimal to negligible increments over time. This strongly supported the efficacy of the animated representation in elucidating saturation dynamics. The consistent recovery percentage over successive time intervals emphasizes the invaluable assistance of the animation's role in facilitating a comprehensive understanding of saturation attainment within the simulated reservoir.

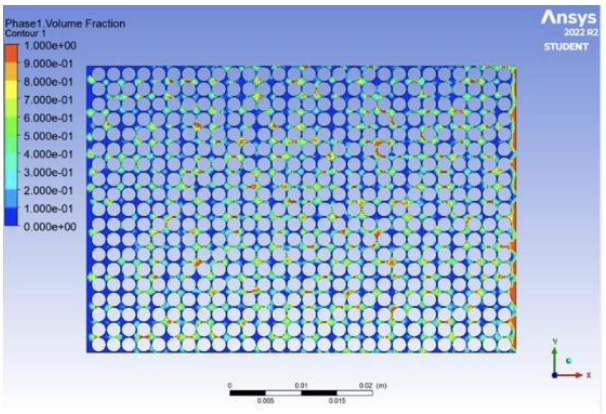

(a) Saturation at 17 s

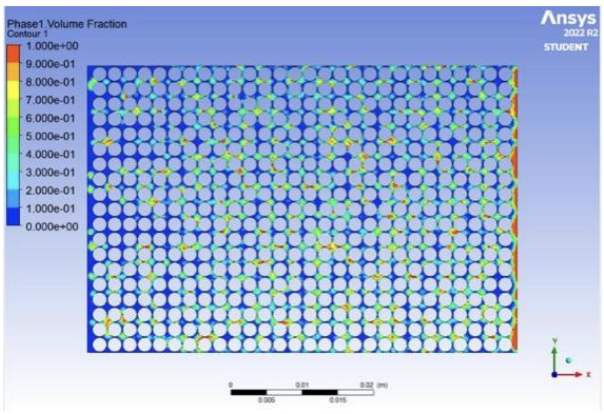

(b) Saturation at 18 s

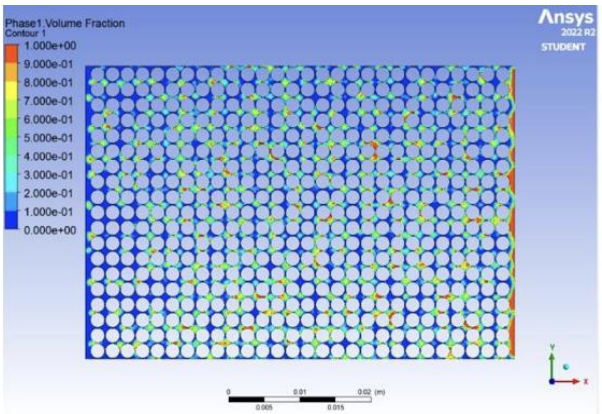

(c) Saturation at 19 s

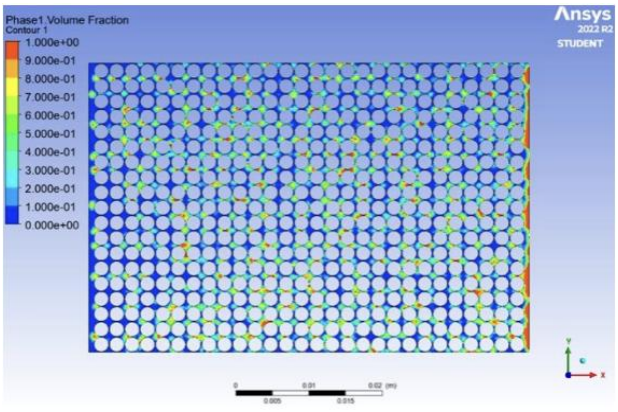

(d) Saturation at 20 s

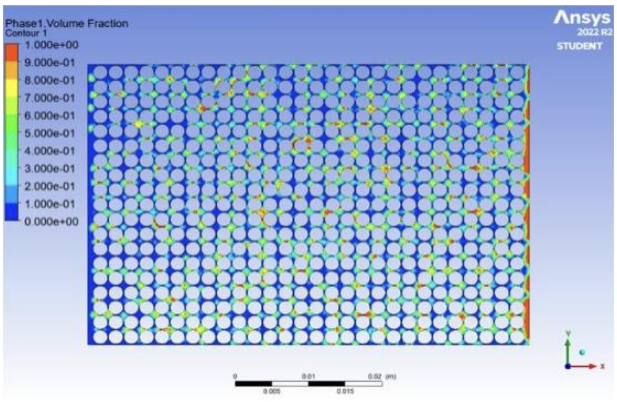

(e) Saturation at 30 s

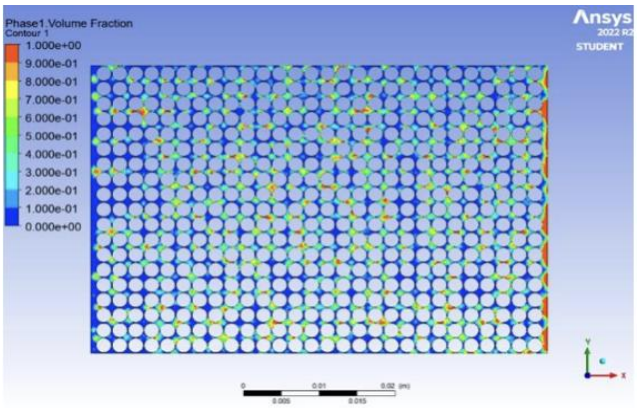

(f) Saturation at 120 s

Figure 3. Saturation at different time steps

9.2 Mesh Independence Check

Upon confirming the saturation of the obtained results, a mesh independence check becomes pivotal in numerical simulations. A mesh independence check is a critical evaluation in numerical simulations to ensure that the results are not significantly affected by changes in mesh density. It involves systematically varying the mesh size or element count while keeping other parameters constant to assess the stability and convergence of the solution. The results for the changes in mesh resolutions, as shown in Tables 8-12, prove that the solution has reached a point where further mesh refinement does not significantly alter the outcome. Achieving independence indicates that the solution is reliable and not heavily reliant on the mesh, ensuring confidence in the simulation's accuracy and validity.

Table 8. Mesh independence test for the model used for validation

Contact Angle	Mesh Element Size	Efficiency
50°	17s	77.45%
50°	18s	77.55%
50°	19s	77.29%
50°	20s	77.47%
50°	30s	76.83%
50°	120s	77.53%

Table 9. Saturation test

Contact Angle	Mesh Element Size	Efficiency
50°	17s	77.45%
50°	18s	77.55%
50°	19s	77.29%
50°	20s	77.47%
50°	30s	76.83%
50°	120s	77.53%

Table 10. Saturation test

Contact Angle	Mesh Element Size	Efficiency
50°	17s	77.45%
50°	18s	77.55%
50°	19s	77.29%
50°	20s	77.47%
50°	30s	76.83%
50°	120s	77.53%

Table 11. Saturation test

Contact Angle	Mesh Element Size	Efficiency
50°	17s	77.45%
50°	18s	77.55%
50°	19s	77.29%
50°	20s	77.47%
50°	30s	76.83%
50°	120s	77.53%

Table 12. Saturation test

Contact Angle	Mesh Element Size	Efficiency
50°	17s	77.45%
50°	18s	77.55%
50°	19s	77.29%
50°	20s	77.47%
50°	30s	76.83%
50°	120s	77.53%

10. MODEL VALIDATION

The average recovery percentage across various mesh sizes can be seen in Table 8, which is 78.92% for the model used for validation. Remarkably, this average remains consistent irrespective of the mesh size used. Notably, the primary study cites a 75% recovery in water-wet media [24]. In the graph shown in Figure 4, the recovery percentages from the reference simulation and experimental data in the paper were compared with the simulation conducted in this study. A noticeable disparity of approximately 20% exists between experimental and validation simulations. This notable difference might be attributed to the mesh independence test, wherein only three simulations were performed, each utilizing a distinct mesh size. These individual tests yielded differing results, as depicted in Table 13. However, the disparity between the simulation in this study and the experimental data is merely around 3%. This discrepancy substantiates the accuracy of the methodology employed for oil extraction, as it closely aligns with experimental observations.

Table 13. Mesh Independence results from the paper used for validation [23]

Grid	Mesh Size (m)	Elements	Nodes	Avg. Velocity (m/s)
1	0.0001	78,334	267,037	0.200
2	0.0010	8,941	7,307	0.014
3	0.0030	8848	13,662	0.056

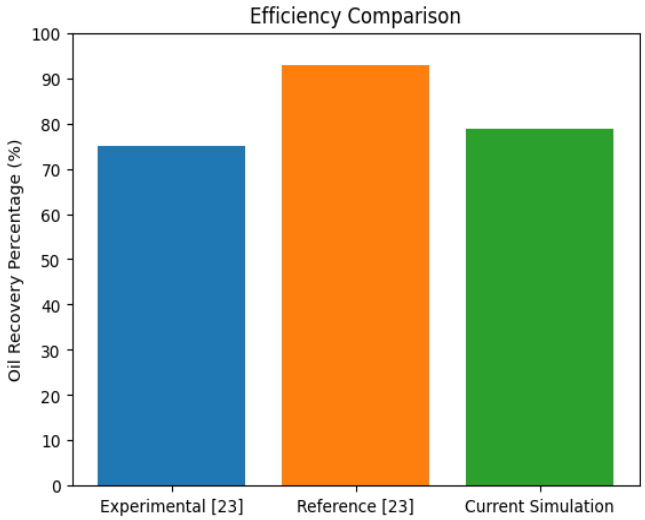

Figure 4. Efficiency comparison (experimental [23], reference paper simulation [23], and this study's simulation)

11. FLOW VISUALIZATION

Figure 5 provides the volume fraction scale used in these visualizations, while the flow visualizations at different time steps for both the proposed model and the validation model are presented in Figures 6 and 7.

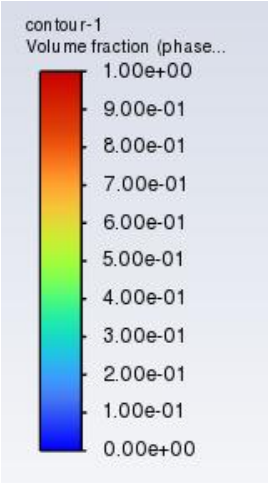

Figure 5. Volume fraction scale for Figure 6 and Figure 7

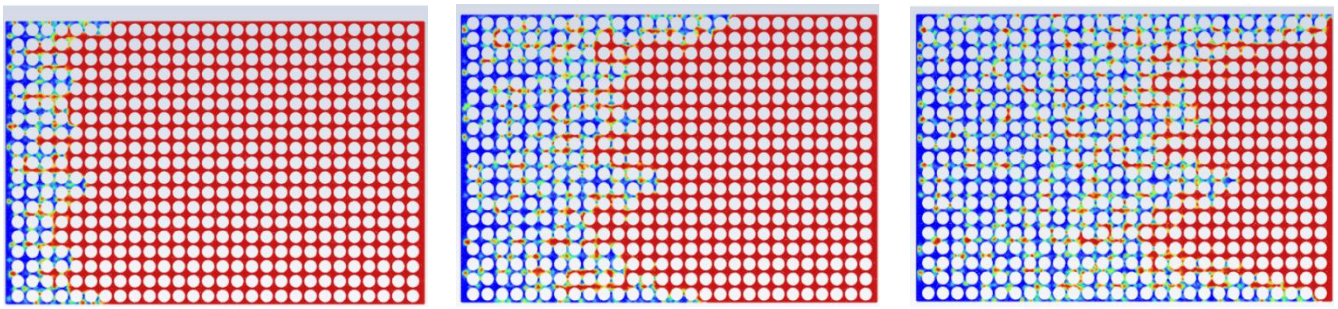

(a) SiO_2 flow at time step 2 (b) SiO_2 flow at time step 5 (c) SiO_2 flow at time step 8

(d) SiO_2 flow at time step 11 (e) SiO_2 flow at time step 15 (f) SiO_2 flow at time step 20

Figure 6. Flow visualizations at different time steps (Validation Model)

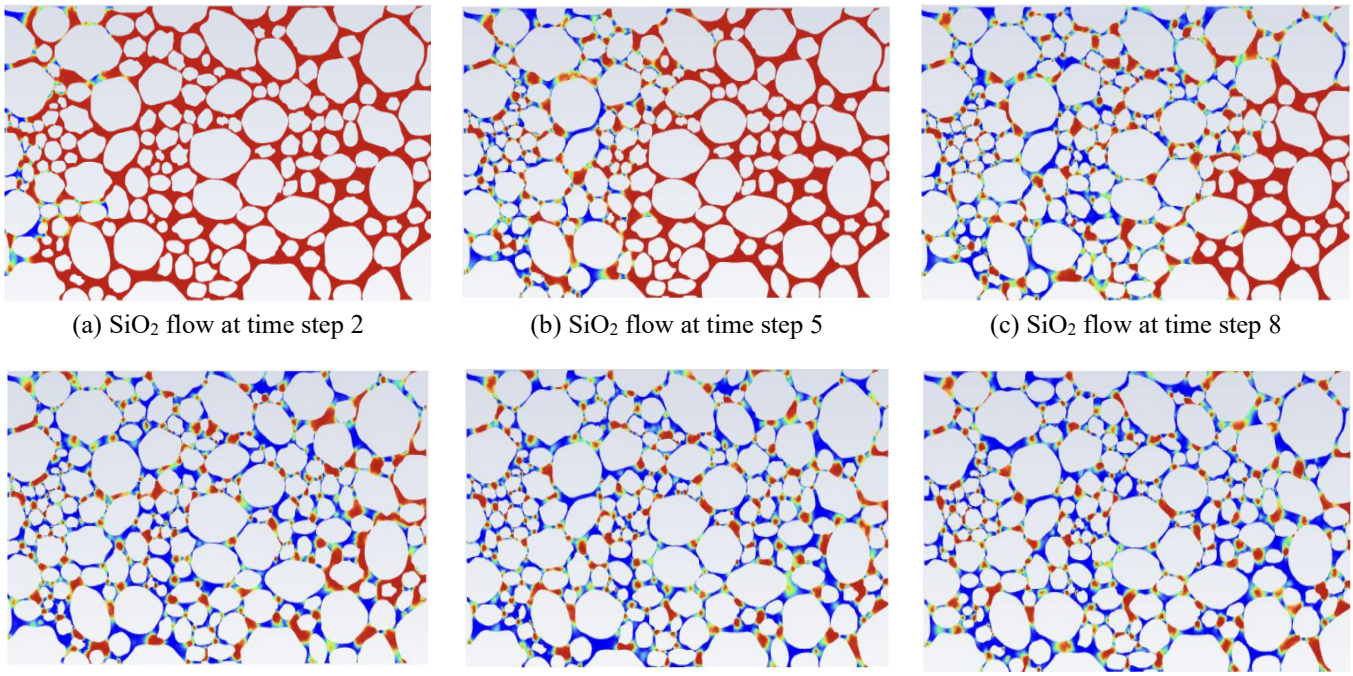

(a) SiO_2 flow at time step 2 (b) SiO_2 flow at time step 5 (c) SiO_2 flow at time step 8

(d) SiO_2 flow at time step 11 (e) SiO_2 flow at time step 15 (f) SiO_2 flow at time step 20

Figure 7. Flow visualizations at different time steps (Proposed Model)

12. STATISTICAL ANALYSIS

Response Surface Methodology (RSM) within the Design of Experiments (DOE) offers a powerful framework for optimizing simulation projects. Its strength lies in systematically exploring how input variables influence the output response of a system. By varying parameters within a limited number of simulations, RSM efficiently navigates the parameter space, identifying optimal combinations that achieve desired outcomes. This approach significantly reduces computational burden while still capturing the intricate relationships between variables and the system response, making it ideal for complex simulations involving numerous parameters. Moreover, RSM enables a deeper understanding of parameter interactions. It illuminates whether variables act independently or synergistically, providing insights into the

relative significance of different parameters. This understanding aids in refining simulation models and determining which factors exert the most substantial influence on the output, guiding subsequent iterations or optimizations.

Furthermore, RSM facilitates the creation of predictive models that capture complex system behaviors. These models extrapolate responses for untested parameter combinations based on observed relationships, streamlining decision-making processes and reducing the need for exhaustive simulations. Additionally, it serves as a validation tool by comparing predicted responses against actual simulation results, ensuring the accuracy and reliability of the model. RSM within DOE emerges as a strategic and efficient approach, with chosen parameters including Interfacial Tension, Contact angle, Velocity, and Nanoparticle Concentration in the base fluid. These parameters play significant roles in nano flooding, influencing the efficiency of EOR processes. Studying and varying these parameters in simulations can help us gauge their individual and collective impacts on oil recovery, optimize the nanofluid composition, and design more effective EOR strategies. This helps in identifying the most suitable conditions for maximizing oil displacement and recovery from reservoirs, advancing the understanding and potential application of nano-flooding in the oil industry. The parameters selected have shown the following importance:

i) Interfacial Tension (Tau): IFT between the injected fluid (nanofluid) and the crude oil is a pivotal parameter in EOR. Lowering the IFT can enhance the displacement of oil from reservoir rocks, aiding in better oil recovery. Nanofluids often have the ability to modify the IFT, and studying their impact through simulation helps understand how effectively the nanofluid can displace the trapped oil.

ii) Contact Angle (Alpha): The contact angle between the fluid and the rock surface influences wettability. Altering the contact angle can affect how the injected fluid interacts with the reservoir rock. Nanoparticles might modify these contact angles, influencing the wetting properties and thus the displacement behavior of fluids within the porous rock matrix.

iii) Velocity (V): Injection velocity determines the flow rate of the injected fluid within the reservoir. It is a critical parameter as it impacts the distribution of the injected fluid and its ability to displace oil. Simulating different velocities allows for an understanding of flow behavior, pressure distribution, and potential alterations in displacement efficiency. 4. Nanoparticle Concentration (Phi): The concentration of nanoparticles in the base fluid affects various properties such as viscosity, density, and thermal conductivity. Optimizing the nanoparticle concentration is crucial as it can impact the mobility and efficiency of the injected fluid in displacing oil from reservoir pores. The range of the parameters taken for the RSM in DOE is shown in Figure 8.

Low and High Values for Factors

Factor	Name	Low	High
A	V	0.001	0.100
B	Phi	0.1	5.0
C	Alpha	0	180
D	Tau	0.000	0.025

Figure 8. Low and high values for parameters considered for DOE

Once the variables were defined for the RSM within Design of Experiments (DOE), the next step is to analyze the results using any statistical tool. For this project, Minitab software was used for statistical analysis. From the software, the following results, as shown in Figures 9-11 and Table 14, were obtained for SiO_2 nanofluid.

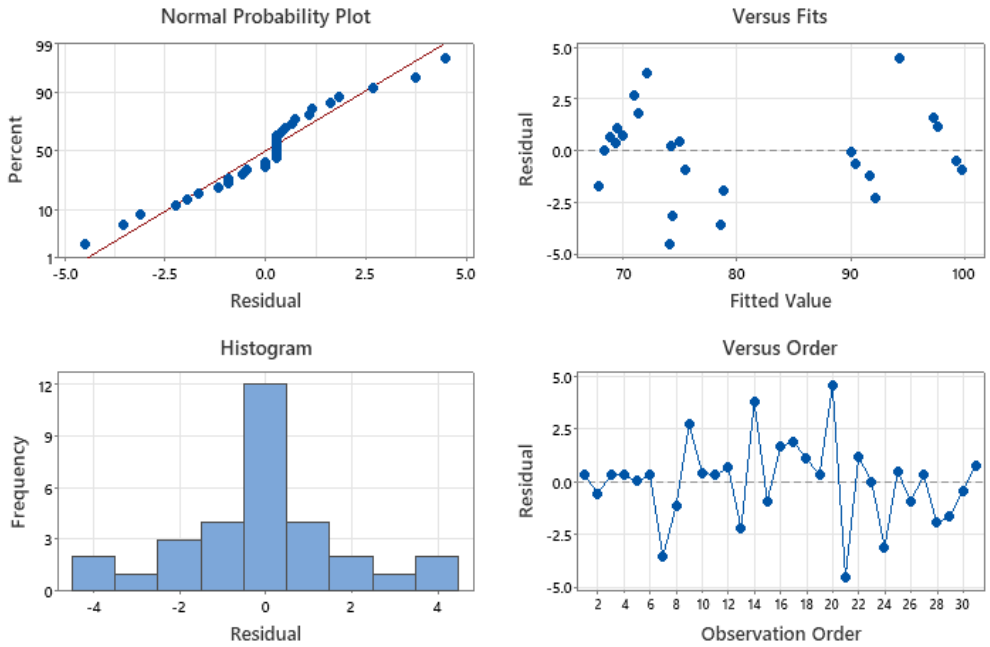

Figure 9. Residual plots for recovery of SiO_2 from Minitab

Table 14. Model summary of SiO_2 from Minitab

Model Summary			
S	R-sq	R-sq(adj)	R-sq(pred)
2.23174	96.83%	95.68%	93.16%

Regression Equation in Uncoded Units for SiO_2 from Minitab:

$$Recovery = 90.21 + 107.1\,V - 0.653\,Phi + 0.0216\,Alpha - 2806\,Tau - 134\,V*V + 0.099\,Phi*Phi - 0.000071\,Alpha*Alpha + 48755\,Tau*Tau + 0.9\,V*Phi - 0.210\,V*Alpha - 2514\,V*Tau + 0.00055\,Phi*Alpha - 5.9\,Phi*Tau - 0.0072\,Alpha*Tau$$

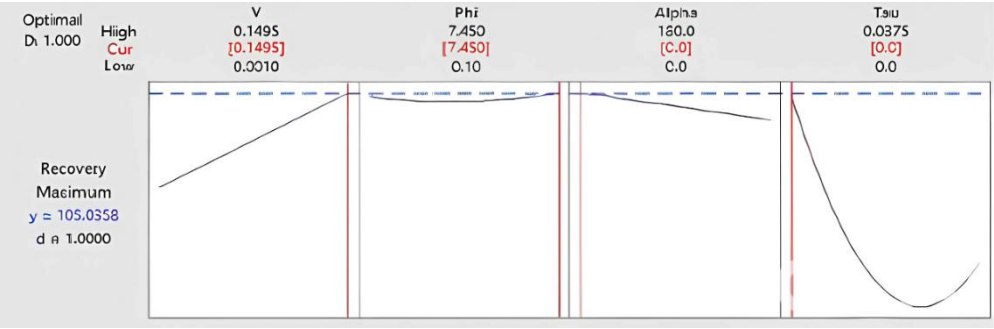

(a) Response optimization: Recovery-SiO_2 from Minitab

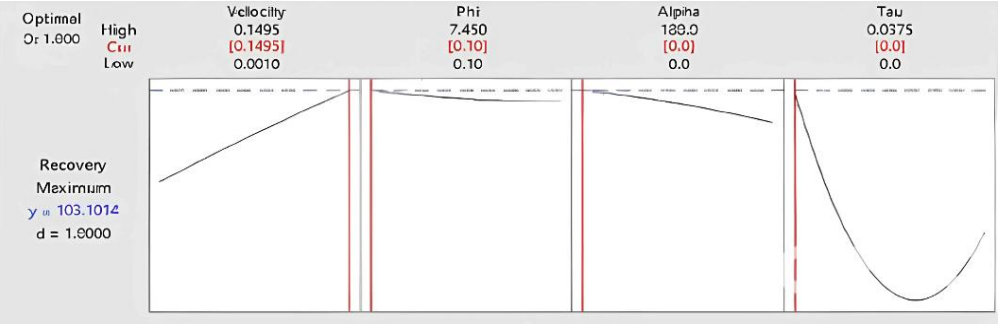

(b) Response optimization: Recovery- Al_2O_3 from Minitab

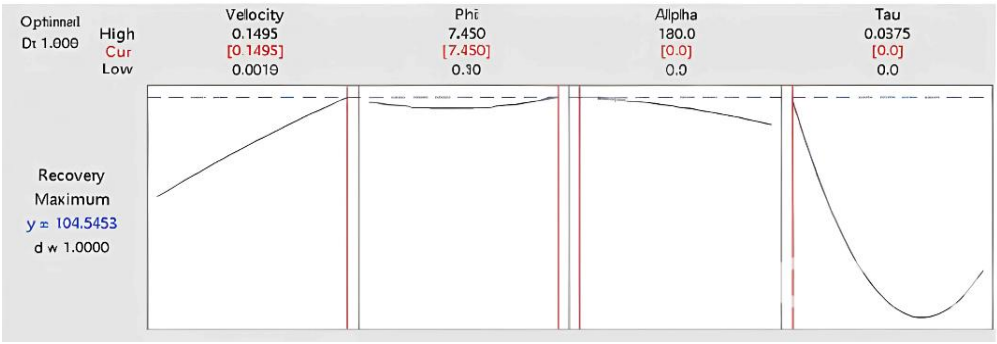

(c) Response optimization: Recovery- CuO from Minitab

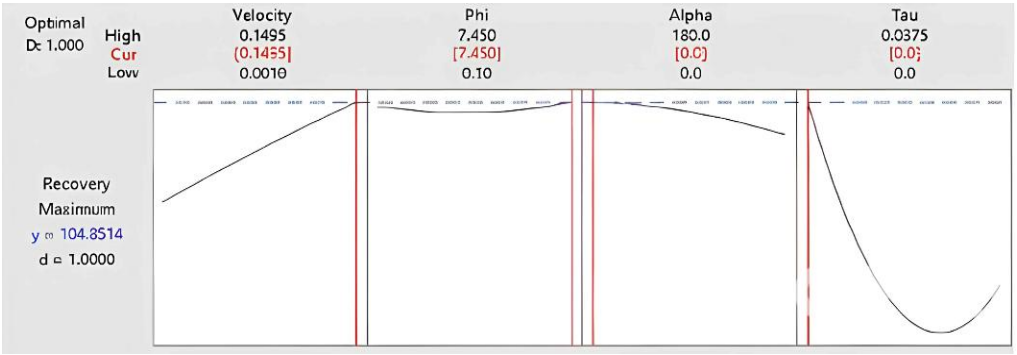

(d) Response optimization: Recovery- TiO_2 from Minitab

Figure 10. Response optimization for the four nanofluids from Minitab

It is important to note that all nanofluids had R-sq and Rsq (adj) above 95%. This allows us to be very confident with the results. The four residual plots of recovery help understand the nature of the analysis. The "normal probability plot" compares predicted values from a regression model against actual experimental data to see how closely they align. It visually evaluates how well the model fits the observed values, aiming for points to cluster around an ideal line representing a perfect fit.

The residuals "versus fits" plot serves to validate the assumption that residuals exhibit random distribution and uniform variability. Ideally, this plot showcases points dispersed around zero without any discernible patterns, indicating the absence of systematic errors within the model. The residual "histogram" offers an overview of their distribution across all observations, particularly effective with a sample size of approximately 20 or more. It serves as a valuable tool for identifying potential skewness or outliers within the residual data. The residuals "versus order" plot organizes residuals based on the data collection sequence. Its role is to examine residual independence. When residuals are independent, their chronological display reveals no noticeable trends or patterns. An ideal scenario shows residuals randomly distributed around the central line, affirming their independence.

All acquired plots align with established statistical expectations, effectively aiding in the thorough assessment of the model's validity and performance. Each plot serves the purpose of validating assumptions, such as independence of residuals, absence of patterns or trends, and identification of potential skewness or outliers, contributing to a robust evaluation of the model's reliability and adherence to statistical principles. The average discrepancy of less than 3% between the regression equation and simulation across 31 runs substantiates the applicability of the regression equation for calculating recovery within the chosen range of variables. This demonstrates the equation's reliability in estimating recovery across various points within the specified variable range.

13. RESPONSE OPTIMIZATION

Figure 10 presents optimized values for all the nanofluids simulated residing within the designated variable range. Notably, an intriguing observation emerges as the highest recorded recovery surpasses the 100% threshold. While theoretically plausible, such outcomes might not align with practical realities in recovery processes. However, this discrepancy serves as a catalyst for a strategic approach, urging the endeavor to maintain variable settings as close as practically feasible to these optimal values. This nuanced strategy aims to navigate the limitations posed by the theoretical bounds, aspiring to achieve recovery rates as high as practically achievable. By focusing on maintaining variable configurations in proximity to these optima, this approach seeks to discern intricate trends and unravel the intricate effects exerted by each variable on the recovery process. The forthcoming analysis in the subsequent sections aims to delve deeper into these observed trends. This rigorous examination will meticulously explore the nuanced relationships between the variables and the resultant recovery rates. By scrutinizing these intricate connections, the goal is to unveil underlying patterns and elucidate the complex interplay among the variables, providing a comprehensive understanding of their collective impacts on the recovery process.

14. TREND ANALYSIS

For generating the trends, the graphs were created for three different conditions. The values of the variables at the three different conditions are:

At average conditions: alpha = 90, v = 0.07525, phi = 3.8, tau = 0.01875

At optimal conditions: alpha = 0, v = 0.1495, phi = 7.5, tau = 0

At close to optimal conditions: alpha = 0, v = 0.1, phi = 7.5, tau = 0.005

Observing the nanoparticle concentration (phi) versus velocity relationship in Figure 11 for the four nanofluids reveals a consistent trend: higher velocities consistently yield increased recovery, regardless of nanofluid concentration. Conversely, lower velocities exhibit higher recovery rates with elevated nanofluid concentrations. This pattern remains mirrored in the velocity versus contact angle analysis, where higher velocities consistently result in enhanced recovery, irrespective of the contact angle. Notably, at intermediate wet medium, there appears to be potential for heightened recovery rates at specific velocity points. Meanwhile, tension demonstrates a more significant impact on recovery than velocity; the lowest tension coupled with the highest velocity produces the highest recovery. Examining contact angle versus concentration suggests an ideal scenario: maintaining higher nanofluid concentrations while keeping the contact angle intermediate across all four nanofluids. The trend observed in tension versus contact angle and concentration remains mostly horizontal, emphasizing tension's dominant effect compared to other parameters. Consistently, maintaining an average tension level while increasing nanofluid concentration, particularly at middle points, seems to foster better recovery outcomes across different nanofluids. These distinct patterns shed light on individual parameters' influence on recovery, offering valuable insights into optimizing recovery rates.

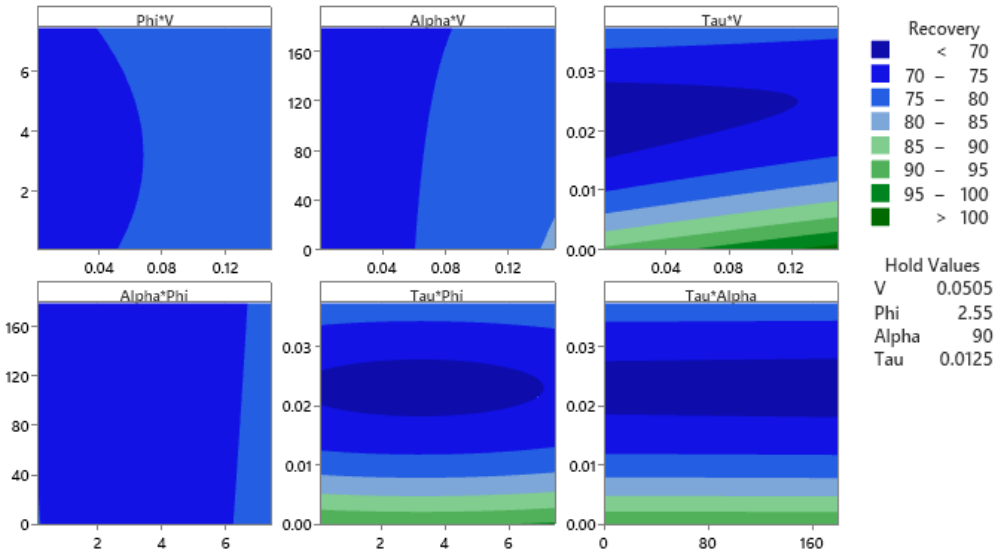

(a) Contour Plots of Recovery-SiO_2 from Minitab

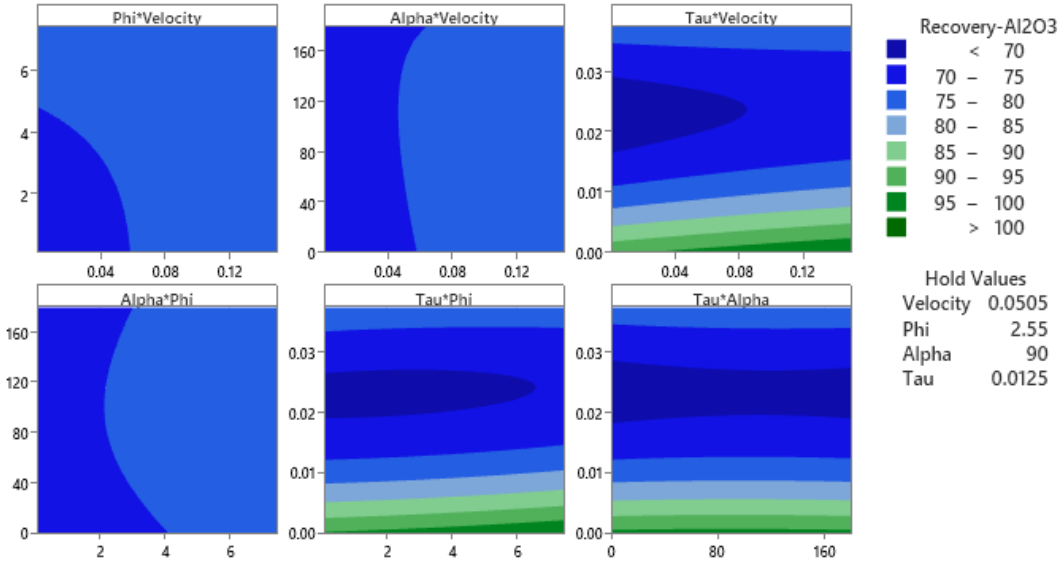

(b) Contour Plots of Recovery-Al_2O_3 from Minitab

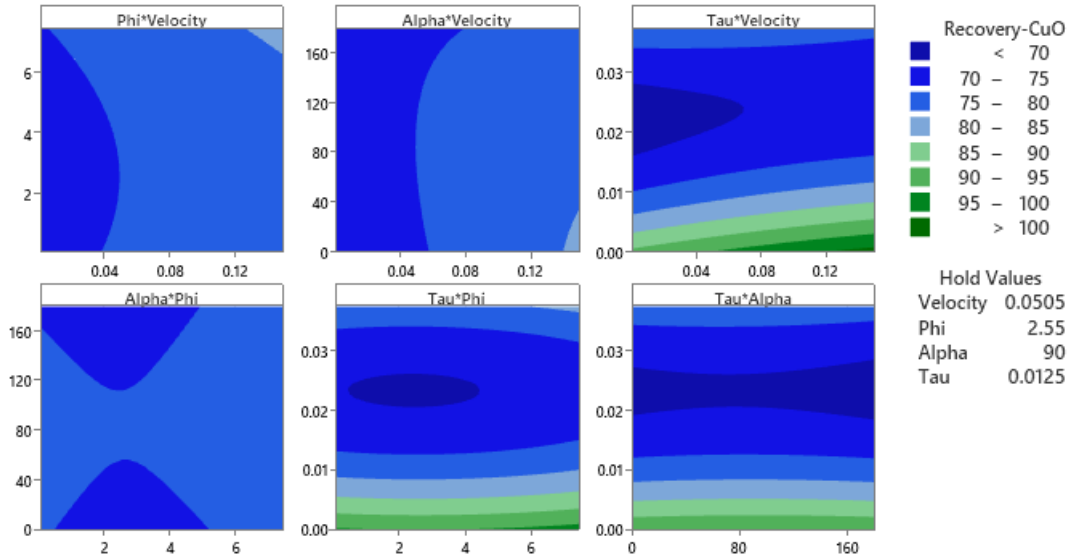

(c) Contour Plots of Recovery-CuO from Minitab

Figure 11. Contour plots for the four nanofluids from Minitab

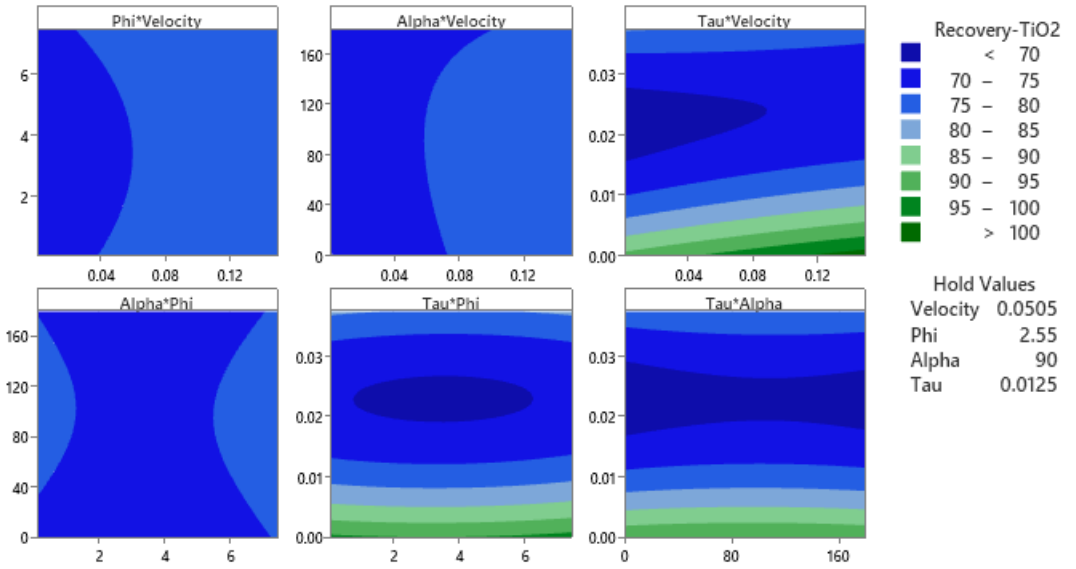

(d) Contour Plots of Recovery-TiO_2 from Minitab

Figure 11. (cont.)

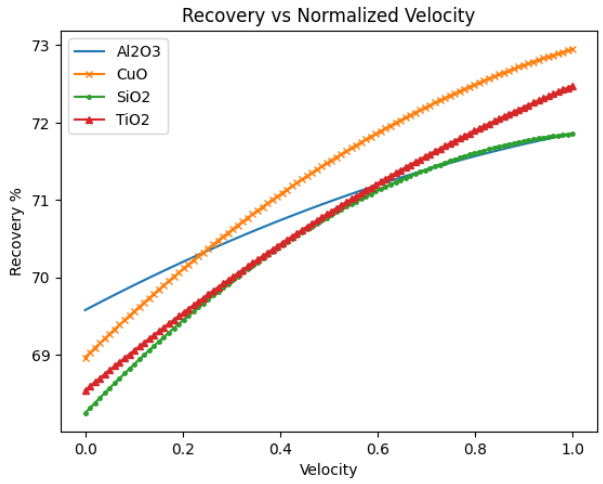

(a) Recovery vs normalized velocity for different

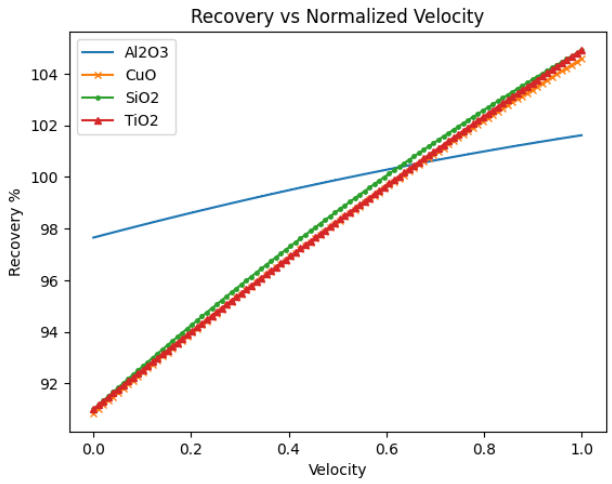

(b) Recovery vs normalized velocity for different

nanofluids at average conditions nanofluids at optimal conditions

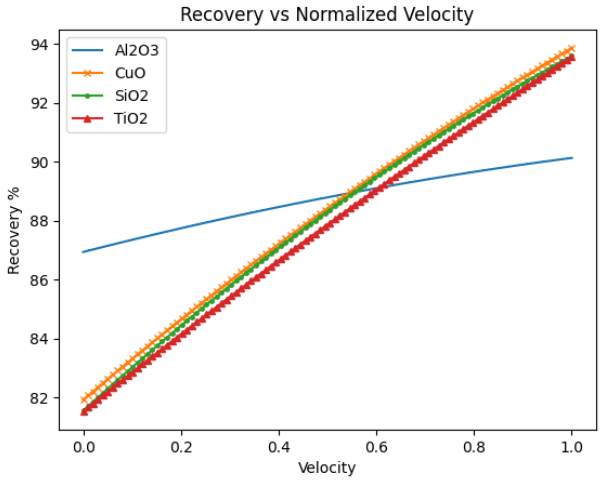

(c) Recovery vs normalized velocity for different nanofluids at close to optimal conditions

Figure 12. Recovery vs Normalized Velocity

In Figure 12, the individual graphs illustrating velocity versus recovery, a notable and consistent trend emerges: higher velocities correspond to increased recovery rates. This phenomenon aligns with the fundamental principles of EOR processes. Higher fluid velocities generally enhance the efficiency within the porous media, facilitating greater contact between the injected nanofluid and trapped oil. This increased interaction enables more effective displacement and mobilization of residual oil, thereby elevating the overall recovery rates. Additionally, higher velocities aid in overcoming reservoir heterogeneities and barriers, further promoting improved oil displacement and recovery. Higher fluid velocities could enhance the dispersion of nanoparticles within the porous media, strengthening their contact and interaction with trapped oil, thus improving the extraction efficiency. This increased dispersion might lead to a more thorough coverage of the porous medium, maximizing oil recovery potential.

Hence, the observed trend of higher recovery rates at elevated velocities is supported by the enhanced fluid flow dynamics facilitating more efficient oil recovery within the EOR framework employing nanofluids which is consistent with the findings of M. Q. Alsedrani [23], who reported that increased injection velocities improve sweep efficiency and nanoparticle distribution, and P. Rostami et al. [24], who observed that higher velocities enhance the detachment of oil droplets from pore walls due to greater shear forces and improved fluid mobility. However, achieving excessively high velocities might pose practical challenges or limitations within real extraction scenarios. Experimental feasibility would necessitate a balance between optimized recovery rates and operational constraints, ensuring that the observed trend aligns with practically attainable fluid velocities.

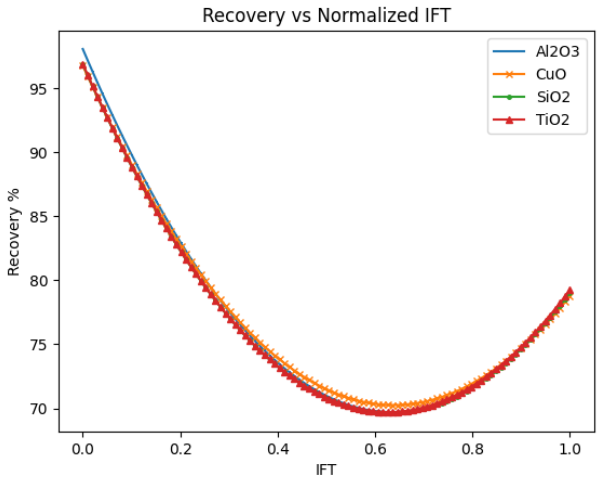

(a) Recovery vs normalized IFT for different nanofluids at average conditions

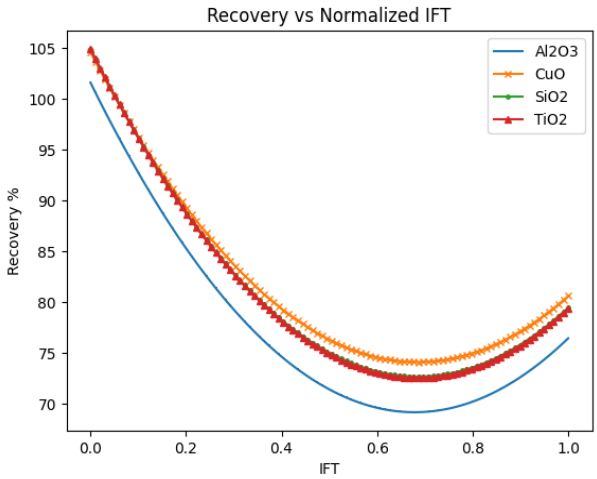

(b) Recovery vs normalized IFT for different nanofluids at optimal conditions

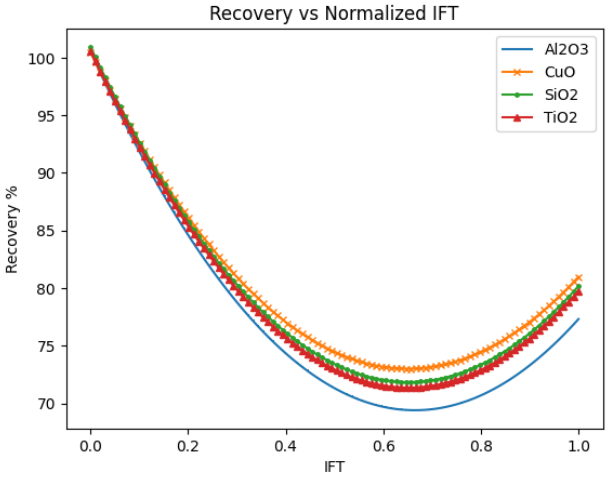

(c) Recovery vs normalized IFT for different nanofluids at close to optimal conditions

Figure 13. Recovery vs Normalized IFT

From Figure 13, the inverse relationship observed between IFT and recovery yields intriguing insights. The trend reflects that as the IFT decreases, indicating reduced resistance between fluids, there is a consistent pattern of increased recovery. This aligns with established principles in EOR processes, where lower IFT values facilitate enhanced mobility and reduced capillary forces within the reservoir, aiding in greater oil displacement, as demonstrated by J. Zhao [33], who found that nanofluids significantly reduced IFT, thereby improving oil mobilization and displacement efficiency, and by A. Ali [22], who showed that decreasing IFT lowered the entry pressure needed for oil to move through pore throats, resulting in higher recovery rates. However, as the IFT progressively increases, a notable decline in recovery is observed. This decline can be attributed to the growing resistance encountered during fluid displacement, hindering efficient oil recovery. Interestingly, after reaching a certain threshold, recovery rates display a slight resurgence, although only to a fraction of the original line. This resurgence might indicate a point where other factors, possibly related to specific reservoir conditions or fluid properties, momentarily favor improved recovery despite higher IFT values. Overall, this observed trend underscores the critical role of IFT in influencing oil recovery, showcasing that while lower IFT consistently facilitates higher recovery, beyond a certain point, the benefits of further IFT reduction diminish, leading to a decline in recovery rates.

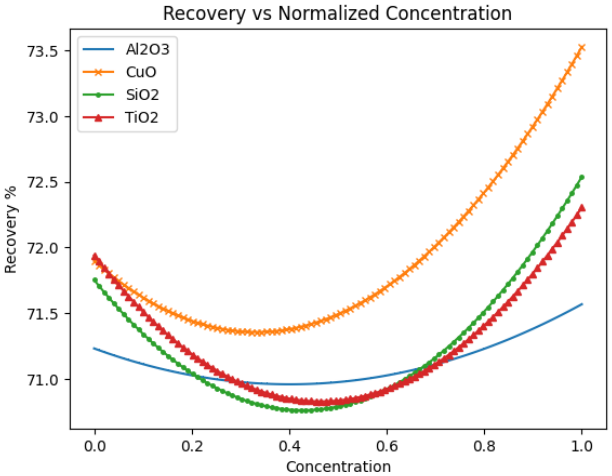

(a) Recovery vs normalized Concentration for different nanofluids at average conditions

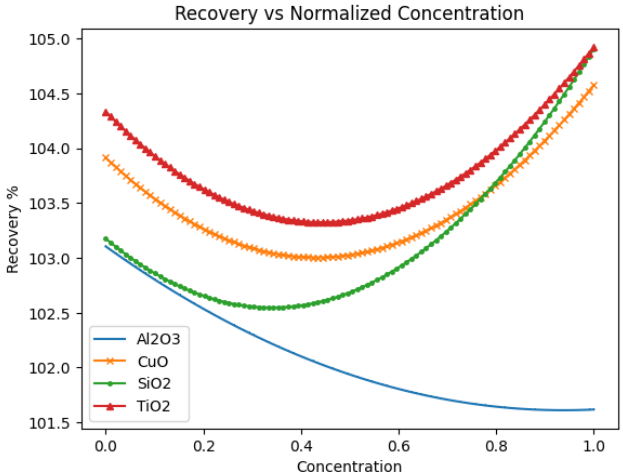

(b) Recovery vs normalized concentration for different nanofluids at optimal conditions

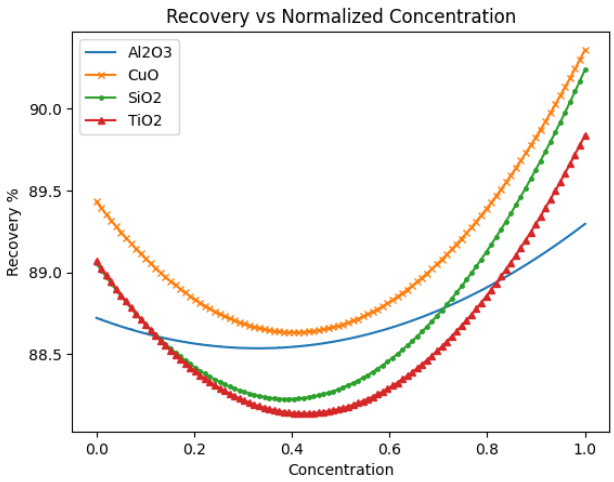

(c) Recovery vs normalized velocity for different nanofluids at close to optimal conditions

Figure 14. Recovery vs Normalized Concentration

The study highlights the nuanced impact of concentration and contact angle on oil recovery, acknowledging their significance despite their comparative importance to velocity and IFT. The concentration trend observed suggests a non-linear relationship between nanofluid concentration and recovery. Initially, as the concentration increases, there is a decline in recovery until a critical point, varying based on the specific nanofluid type, where further concentration incrementally enhances recovery rates. This closely resembles a U-shaped trend, indicating an optimal concentration range for maximizing recovery.

Moreover, an intriguing observation in Figure 14(b), pertaining to Al_2O_3 nanofluid, reveals an anomalous trend. This anomalous trend contradicts the typical expectation that increasing nanoparticle concentration often correlates with improved recovery. This unusual pattern might signify a potential issue at play. It's likely that at extremely low nanoparticle concentrations (depicted as zero concentration in the graph), other factors or interactions within the system might be optimizing the recovery process. This anomaly might indicate that at negligible nanoparticle concentrations, other fluid properties or reservoir conditions could be more conducive to efficient oil recovery. Further investigation is warranted to comprehend this unexpected behavior fully. Detailed analysis considering the fluid's behavior, reservoir characteristics, or potential interactions at very low nanoparticle concentrations would be crucial in deciphering this unusual trend and its implications in optimizing recovery under specific conditions.

As suggested in the study by Sepehri, M. et al. [34], this behavior can stem from dominant interfacial or capillary forces at very low concentrations, where minimal nanoparticle presence might still enhance wettability or reduce IFT slightly, leading to unexpectedly efficient displacement under certain conditions. In general, under varied conditions, aiming for the highest feasible nanofluid concentration remains an ideal strategy for optimizing recovery rates, although careful evaluation and validation of this approach across diverse scenarios are crucial.

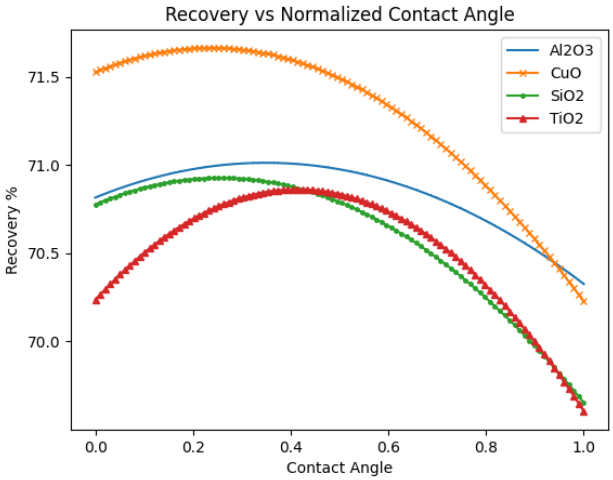

(a) Recovery vs normalized contact angle for different nanofluids at average conditions

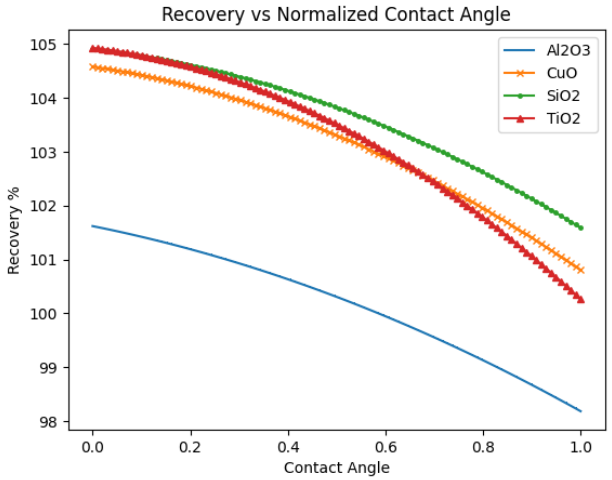

(b) Recovery vs normalized contact angle for different nanofluids at optimal conditions

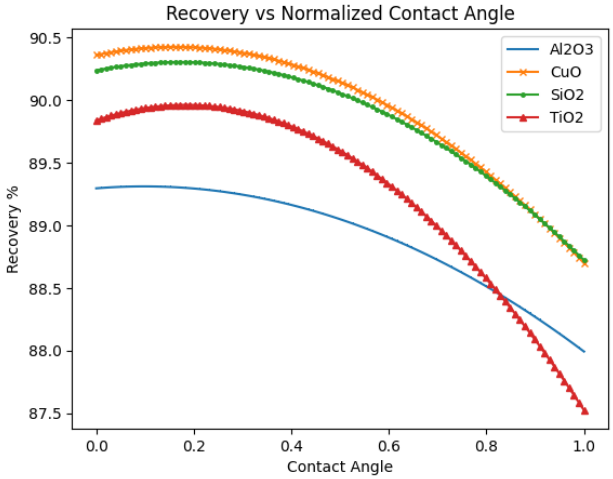

(c) Recovery vs normalized contact angle for different nanofluids at close to optimal conditions

Figure 15. Recovery vs Normalized concentration of Nanofluids

The relationship between contact angle and recovery is intricate, where the contact angle might appear constant but can be influenced by various factors. The trend observed in contact angle versus recovery showcases a crucial point: the optimal contact angle for maximizing recovery is not universally fixed; instead, it can vary based on specific conditions. Depending on the unique circumstances, the optimal contact angle might align with either water-wet or intermediate-wet conditions. This divergence is apparent in different studies where contradictory optimal angles are reported. Such variability is entirely possible and justifiable because these outcomes are contingent upon the distinct experimental or simulation conditions employed in each study. For instance, the study by Chau et al. [35] demonstrated that changes in contact angle directly influenced the wettability alteration effect of nanofluids, and that this alteration significantly affected capillary pressure and relative permeability, thus impacting oil recovery. This discrepancy underscores the sensitivity of contact angle influence on recovery to the specific parameters and conditions explored in each study. It emphasizes the importance of recognizing that optimal contact angles are context-dependent, requiring a nuanced approach tailored to the distinct conditions of each study.

While the simulation results provide valuable insights into the effects of IFT reduction, wettability alteration, and fluid velocity on oil recovery, it is important to acknowledge inherent limitations and uncertainties. Pore-scale models often simplify complex reservoir heterogeneities, and assumptions regarding fluid properties and boundary conditions can influence accuracy. Furthermore, scaling these findings to field-scale operations requires caution due to variations in reservoir geology, temperature, and pressure. Despite these challenges, the demonstrated mechanisms—such as enhanced nanoparticle dispersion at higher velocities and combined wettability/IFT effects—offer promising avenues for improving EOR strategies. Practical implementation must consider optimal injection rates and nanoparticle concentrations to balance efficiency with operational constraints, minimizing risks like formation damage or nanoparticle aggregation. Future work should focus on integrating more realistic reservoir conditions and validating simulations with core flooding or field pilot tests to enhance reliability for industrial applications.

15. CONCLUSION

This study ensured the accuracy of its findings by conducting numerical simulations that closely mirrored real-world conditions through stringent model validation. This comprehensive validation ensured confidence in the precision and reliability of the numerical approach. The simulation incorporated initial crude oil saturation (Swi = 0), two-phase laminar flow conditions, a constant injection velocity of 0.004 m/s, interfacial tension of 0.015 N/m, and a contact angle of 50°, all based on experimental values, to dynamically study displacement phenomena over time and for model validation. Exploring the domain of key parameters influencing oil recovery, which included the velocity, interfacial tension, concentration, and contact angle, the investigation unraveled multifaceted insights. Consistently, the study showed that achieving higher velocities helps extract more oil, showing how essential velocity is in displacing the oil effectively. It also found that the reduced interfacial tension facilitates increased oil recovery. These trends were clearly reflected in the recovery performance curves, where increasing velocity and reducing interfacial tension showed consistent improvements in oil recovery. The study revealed a noteworthy aspect concerning the relationship between nanofluid concentration and oil recovery. It identified specific concentration thresholds crucial for optimal recovery. It identified specific concentration thresholds as optimal, before which recovery did not improve, suggesting diminishing returns possibly due to nanoparticle behavior such as aggregation.

However, in the midst of these findings, the study unveiled interesting variations in contact angle optimization, emphasizing its subtle and context-specific impact on recovery outcomes. This comprehensive understanding of parameter effects, supported by rigorous validation, not only contributes to the fundamental comprehension of nanofluid-

assisted recovery but also presents a range of possibilities for further exploration and advancement in the understanding of oil recovery techniques. Serving as a foundational pillar, this study provides the groundwork to refine and advance nanofluid-assisted recovery methods. Subsequent studies could explore diverse reservoir properties, varied nanoparticle compositions, or analyze different environmental implications. These endeavors collectively aim to advance enhanced oil recovery strategies.

ACKNOWLEDGEMENTS

The authors would like to thank the School of Engineering and Physical Sciences, Heriot-Watt University, Dubai, UAE for the facility and support. Besides, appreciation to all those whose direct or indirect contributions have played a part in the completion of this research.

CONFLICT OF INTEREST

The authors confirm that there is no conflict of interest related to the manuscript.

AUTHOR CONTRIBUTIONS

Krishna Priya carried out the conceptualization, methodology, investigation, data curation, formal analysis, visualization, and preparation of the original draft.

Ahmed N Oumer provided supervision, contributed to data analysis by reviewing the process, and participated in reviewing the manuscript.

REFERENCES

[1] R. Lukasz, "History of Oil - A timeline of the modern oil industry," EKT Interactive, Oct. 19, 2023. Available: https://ektinteractive.com/history-of-oil/

[2] U. Ali, "The history of the oil and gas industry from 347 AD to today," Offshore Technology, Mar. 07, 2019. [Online]. Available: https://www.offshore-technology.com/comment/history-oil-gas/

[3] Anton Paar Wiki, "Enhanced Oil Recovery," [Online]. Available: https://wiki.anton-paar.com/en/enhanced-oil-recovery/.

[4] Rigzone, "What Is EOR, and How Does It Work?" [Online] Available: https://www.rigzone.com/training/insight/?insight id=313

[5] North Sea Transition Authority, "Enhanced Oil Recovery," [Online]. Available: https://www.nstauthority.co.uk/regulatory-information/-explorationand-production/development/enhanced-oil-recovery/.

[6] Department of Energy, "The Economic Benefits of Oil & Gas" [Online]. Available: https://www.energy.gov/articles/economic-impact-oil-and-gas

[7] UKOG, "Why oil is important" [Online]. Available: https://www.ukogplc.com/page.php?pID=74

[8] A. Ahmadi, A. K. Manshad, J. A. Ali, S. Iglauer, S. M. Sajadi, A. Keshavarz, et al., "Insight into nano-chemical enhanced oil recovery from carbonate reservoirs using environmentally friendly nanomaterials," *ACS Omega*, vol. 7, no. 41, pp. 36165–36174, 2022.

[9] A. A. Franco, C. Franco, R. D. Zabala, I. Bahamon, A. M. Forero, and F. B. Cortes, "Field applications of nanotechnology in the oil and gas industry: Recent advances and perspectives," *Energy & Fuels*, vol. 35, no. 23, pp. 19266–19287, 2021.

[10] Y. Sun, D. Yang, L. Shi, H. Wu, Y. Cao, Y. He, et al., "Properties of nanofluids and their applications in enhanced oil recovery: A comprehensive review," *Energy & Fuels*, vol. 34, no. 2, pp. 1202–1218, 2020.

[11] Z. Hu, M. A. Haruna, H. Gao, E. Nourafkan, and D. Wen, "Rheological properties of partially hydrolyzed polyacrylamide seeded by nanoparticles," *Industrial & Engineering Chemistry Research*, vol. 56, no. 12, pp. 3456–3463, 2017.

[12] M. Iravani, Z. Khalilnezhad, and A. Khalilnezhad, "A review on application of nanoparticles for EOR purposes: history and current challenges," *Journal of Petroleum Exploration and Production Technology*, vol. 13, no. 4, pp. 959–994, 2023.

[13] M. Y. Kanj, M. H. Rashid, and E. P. Giannelis, "Industry first field trial of reservoir nanoagents," in *SPE Middle East oil and Gas Show and Conference*, pp. SPE-142592

[14] Y. Kazemzadeh, S. Shojaei, M. Riazi, and M. Sharifi, "Review on application of nanoparticles for EOR purposes: A critical review of the opportunities and challenges," *Chinese Journal of Chemical Engineering*, vol. 27, no. 2, pp. 237–246, 2019.

[15] A. M. S. Ragab and A. E. Hannora, "A comparative investigation of nano particle effects for improved oil recovery – Experimental work," in *SPE Kuwait Oil and Gas Show and Conference*, pp. SPE-175395, 2015.

[16] R. Jiang, K. Li, and R. N. Horne, "A mechanism study of wettability and interfacial tension for EOR using silica nanoparticles," In *SPE Annual Technical Conference and Exhibition*, p. D031S046R003, 2017.

[17] M. B. Khan, M. F. Khoker, M. Husain, M. Ahmed, and S. Anwer "Effects of nanoparticles on rheological behavior of polyacrylamide related to enhance oil recovery," *Academic Journal of Polymer Science*, vol. 1, no. 5, p. 555573, 2018.

[18] R. Gharibshahi, A. Jafari, A. Haghtalab, and M. S. Karambeigi, "Application of CFD to evaluate the pore morphology effect on nanofluid flooding for enhanced oil recovery," *RSC Advances*, vol. 5, no. 37, pp. 28938–28949, 2015.

[19] M. Iravani, Z. Khalilnezhad, and A. Khalilnezhad, "A review on application of nanoparticles for EOR purposes: history and current challenges," *Journal of Petroleum Exploration and Production Technology*, vol. 13, no. 4, pp. 959–994, 2023.

[20] T. Huang, B. A. Evans, J. B. Crews, and C. K. Belcher, "Field case study on formation fines control with nanoparticles in offshore wells," in *SPE Annual Technical Conference and Exhibition*, pp. SPE-135088, 2010.

[21] Y. Kaito, A. Goto, D. Ito, S. Murakami, H. Kitagawa, and T. Ohori, "First nanoparticle-based EOR nano-EOR project in Japan: Laboratory experiments for a field pilot test," in *SPE Improved Oil Recovery Conference*, p. D011S008R001, 2022.

[22] A. R. I. Ali and B. Salam, "A review on nanofluid: Preparation, stability, thermophysical properties, heat transfer characteristics and application," *SN Applied Sciences*, vol. 2, no. 10, p. 1636, 2020.

[23] M. Q. Alsedrani and G. T. Chala, "Investigation of the effects of silica nanofluid for enhanced oil recovery applications: CFD Simulation study," *Arabian Journal for Science and Engineering*, vol. 48, no. 7, pp. 9139–9158, 2022.

[24] P. Rostami, M. Sharifi, B. Aminshahidy, and J. Fahimpour, "The effect of nanoparticles on wettability alteration for enhanced oil recovery: Micromodel experimental studies and CFD simulation," *Petroleum Science*, vol. 16, no. 4, pp. 859–873, 2019.

[25] Y. Zhou, W. Guan, C. Zhao, H. Hu, Z. He, X. Zou et al., "A computational workflow to study CO_2 transport in porous media with irregular grains: Coupling a Fourier series-based approach and CFD," *Journal of Cleaner Production*, vol. 418, p. 138037, 2023.

[26] M. W. Clark, "Quantitative shape analysis: A review," *Journal of the International Association for Mathematical Geology*, vol. 13, no. 4, pp. 303–320, 1981.

[27] D. Su and Y. Wang, "Quantification of angularity of general-shape particles by using Fourier series and a gradient-based approach," *Construction and Building Materials*, vol. 161, pp. 547–554, 2018.

[28] Y. Ahmadi, M. Hassanbeygi, and R. Kharrat, "The effect of temperature and injection rate during water flooding using carbonate core samples: An experimental approach," *Iranian Journal of Oil and Gas Science and Technology*, vol. 5, no. 4, pp. 18–24, 2016.

[29] P. P. Y. A. Jacinta, M. F. Majnis, and S. A. Musa, "CFD simulation of the oil displacement in micromodel for enhanced oil recovery application," *IOP Conference Series: Materials Science and Engineering*, vol. 1092, no. 1, p. 012011, 2021.

[30] B. Barbes, R. Paramo, E. Blanco, and C. Casanova, "Thermal conductivity and specific heat capacity measurements of CuO nanofluids," *Journal of Thermal Analysis and Calorimetry*, vol. 115, no. 2, pp. 1883–1891, 2013.

[31] M. H. Esfe, A. Karimipour, W. Yan, M. Akbari, M. R. Safaei, and M. Dahari, "Experimental study on thermal conductivity of ethylene glycol based nanofluids containing Al_2O_3 nanoparticles," *International Journal of Heat and Mass Transfer*, vol. 88, pp. 728–734, 2015.

[32] M. H. Esfe, A. A. Nadooshan, A. Arshi, and A. Alirezaie, "Convective heat transfer and pressure drop of aqua based TiO_2 nanofluids at different diameters of nanoparticles: Data analysis and modeling with artificial neural network," *Physica E: Low-Dimensional Systems and Nanostructures*, vol. 97, pp. 155–161, 2018.

[33] J. Zhao and D. Wen, "Pore-scale simulation of wettability and inter facial tension effects on flooding process for enhanced oil recovery," *RSC Advances*, vol. 7, no. 66, pp. 41391–41398, 2017.

[34] M. Sepehri, B. Moradi, A. Emamzadeh, and A. H. Mohammadi "Experimental study and numerical modeling for enhancing oil recovery from carbonate reservoirs by nanoparticle flooding," *Oil & Gas Science and Technology – Revue d'IFP Energies nouvelles*, 74, p. 5, 2019.

[35] T. T. Chau, W. J. Bruckard, P. T. L. Koh, and A. V. Nguyen, "A review of factors that affect contact angle and implications for flotation practice," *Advances in Colloid and Interface Science*, vol. 150, no. 2, pp. 106–115, 2009.